Experimental and theoretical characterization of commercial nanofiltration membranes for the treatment of ion exchange spent regenerant

Micari, M.; Diamantidou, D.; Heijman, B.; Moser, M.; Haidari, A.; Spanjers, H.; Bertsch, V.

DOI
10.1016/j.memsci.2020.118117

Publication date
2020

Document Version
Final published version

Published in
Journal of Membrane Science

Journal of Membrane Science 606 (2020) 118117

Contents lists available at ScienceDirect

Journal of Membrane Science

journal homepage: http://www.elsevier.com/locate/memsci

Experimental and theoretical characterization of commercial nanofiltration membranes for the treatment of ion exchange spent regenerant

M. Micari [a,*], D. Diamantidou [b], B. Heijman [c], M. Moser [a], A. Haidari [c], H. Spanjers [c], V. Bertsch [a,d]

[a] German Aerospace Center (DLR), Institute of Engineering Thermodynamics, Department of Energy System Analysis, Pfaffenwaldring 38-40, 70569, Stuttgart, Germany
[b] Lenntech, Water Treatment Solutions, Distributieweg 3, 2645 EG, Delfgauw, The Netherlands
[c] Delft University of Technology, Department of Water Management, Stevinweg 1, 2628 CN, Delft, The Netherlands
[d] Ruhr-Universität Bochum, Chair of Energy Systems and Energy Economics, Universitätsstr. 150, 44801, Bochum, Germany

ARTICLE INFO

Keywords:
Nanofiltration
Wastewater treatment
Membrane characterization
Ionic rejection
Water softening

ABSTRACT

This work presents a joint experimental and simulation campaign aimed at characterizing two nanofiltration membranes (TS80 and NF270) in the presence of a multi-ionic water solution simulating the spent regenerant of cationic ion exchange resins employed for water softening. We identified the membrane parameters, which allowed for predicting the performances through the Donnan Steric Pore Model with Dielectric Exclusion. A good agreement between model and experimental trends of rejection as a function of the applied pressure was observed (error < 15%). The analysis of trans-membrane fluxes and exclusion coefficients showed that dielectric exclusion was the crucial mechanism for the ionic partition. In fact, the lower pore dielectric constant found for TS80 justified the higher rejections to divalent cations with respect to NF270. Moreover, negative charge densities were found for both membranes, because of the high concentration of chloride ions in the feed, which likely adsorbed onto the membrane. However, it was observed that the experimental rejections did not change significantly with the feed pH. This result, in line with the minor role of the Donnan exclusion resulting from the model, suggested that the membrane performances were not much affected by the charge density at high feed ionic strengths (~1 M).

1. Introduction

Nanofiltration (NF) is a membrane technology widely used as a treatment process or as a pre-treatment step in various industrial sectors, for its ability to selectively separate multivalent ions from water solutions. The performances of NF membranes are intermediate between those of Reverse Osmosis (RO) and Ultrafiltration, their pore size is in the order of 1 nm [1] and their molecular weight cut-off (MWCO) typically ranges between 100 and 1000 Da [2,3]. NF membranes constitute selective barriers to remove various compounds, such as organics, inorganic metal ions and microorganisms, thanks to the combination of three exclusion mechanisms: steric, Donnan and dielectric exclusion [4]. Therefore, various industrial applications of NF are reported in the literature, which concern the concentration and separation of specific components or the fractionation of a liquid solution into two at different concentrations [5].

NF is widely used in environmental applications and in particular, for the production of high-quality water from groundwater, surface water and wastewater [6]. In this context, extensive research has been carried out on the removal of arsenic (As) and pesticides from groundwater [7,8] and on the removal of natural organic matter, dissolved organic carbon and heavy metals from surface water [9].

Furthermore, NF is used to treat various industrial wastewater effluents and in particular, to remove ions and compounds from waste streams. In the textile industry, for instance, NF is employed to treat the spent dyeing solution produced by the industrial process, to separate dye and salts (NaCl and Na_2SO_4) [10,11] and to remove the colour and enable the reuse of the permeate as fresh reactant solution [12–14]. Other applications of NF include the removal of heavy metals such as barium, strontium [15], cadmium, nickel [16] and lead [17] from wastewater, the removal of lithium from salt lake brines [18], the recovery of boric acid present in radioactive wastewater produced by nuclear power plants [19] and the treatment of acidic coal mine drainage [20].

* Corresponding author.
E-mail address: Marina.Micari@dlr.de (M. Micari).

https://doi.org/10.1016/j.memsci.2020.118117
Received 17 December 2019; Received in revised form 13 March 2020; Accepted 31 March 2020
Available online 5 April 2020

Within the food industry, NF is widely applied in the beverage industry for juice concentration [21] and in the dairy industry for lactose recovery and whey demineralization [22,23]. Another industrial food sector that uses membrane processes is the sugar industry, where NF is used to treat the sugar beet press water [24] or to purify and recover the brine produced by the regeneration of the ion exchange resins used for sugar decolourisation [25].

In the water industry, NF has found several applications in water softening and typically as a pre-treatment of desalination processes. The use of NF reduces the risks of scaling and fouling in downstream equipment by removing divalent ions and organic compounds, and it leads to a decrease in the osmotic pressure of the solution [26]. Different integrated systems have been evaluated, which present (i) the coupling of NF with other membrane desalination processes, such as RO or Electrodialysis and (ii) the coupling of NF with thermal processes, as multi-effect distillation or multi-stage flash (MSF) [27]. Concerning the integration of NF with membrane processes, the decrease of the osmotic pressure due to the NF pre-treatment corresponds to an enhancement of the available driving force at the same applied pressure and, consequently, to an increase of the water recovery in the desalination unit [28]. With this regard, the Saline Water Conversion Corporation proposed the employment of NF as a pre-treatment step for seawater RO and relevant works in the literature showed that the water recovery increases by 60% and the cost decreases by about 30% [29,30]. Regarding the integration of NF with thermal processes, the removal of divalent ions, and in particular of calcium and sulphate ions, allows for operating at higher temperatures in the desalination unit. Some authors presented NF-MSF systems with MSF operating at a Top Brine Temperature (TBT) of 120 °C without any scaling [31].

Another application of NF within the water industry concerns the treatment of the spent brine produced by the regeneration of ion exchange resins. Ion exchange resins are employed in various sectors and the composition of the spent solution produced by the regeneration of the resins depends on the application. For example, NF has been used to remove the Natural Organic Matter from the spent regenerant of the resins used in municipal wastewater purification [32] or to purify the effluent produced by the resins used for sugar decolourisation [5,25]. In this work, we deal with the effluent produced by the regeneration of resins employed for water softening. In particular, this work aims at characterizing NF membranes in the presence of an artificial brine simulating the industrial effluent, containing magnesium and calcium ions and sodium chloride. The characterization is fundamental to be able to simulate the NF unit within an integrated treatment system (chain). The treatment chain is devised in order to recover raw materials and recycle the purified effluent to the industrial process. In particular, NF is used as the first treatment step to separate magnesium and calcium from the NaCl-rich solution that can be concentrated and recycled to the regeneration process. Conversely, the concentrate solution produced by the NF, which includes magnesium and calcium ions, is further treated to produce crystals of $Ca(OH)_2$ and $Mg(OH)_2$. The latter is identified by the European Commission as a critical raw material [33]. Therefore, NF plays a crucial role in the brine treatment process, since a highly-performing separation step leads to an almost total recovery of the divalent ions in the form of hydroxides, which is crucial for the economic profitability of the process [34].

Given the importance of the NF unit in the treatment chain described above, it is fundamental to predict accurately the NF membrane behaviour by introducing suitable calibration parameters obtained via a full characterization of the membranes.

The characterization of NF membranes has been a very active field of research in the last twenty years. Membranes are typically described as charged porous structures, characterized by parameters including pore radius (r_p), active layer membrane thickness (δ_m), dielectric constant within the pores (ε_{pore}) and charge density (X_D). Various methods have been proposed in the literature for characterization purposes. Among these, direct methods include atomic force microscopy to estimate the pore size on the membrane surface [35] and membrane surface zeta potential, used as a measure of the Donnan potential [36]. Conversely, indirect methods consist in the combination of experimental measurements of neutral and ionic solutes rejection and model simulations [37].

As far as the modelling is concerned, the first model, proposed by Spiegler and Kedem, was based on irreversible thermodynamics and considered the membrane as a black box, where the membrane porosity was neglected [38]. Later, Tsuru et al. proposed a model based on the extended Nernst-Planck equation [39], which was followed by two other models: the space charge model and the Teorell-Meyer-Sievers model [40]. Finally, Bowen et al. proposed the Donnan Steric Pore Model (DSPM) that was able to predict the NF performances with neutral solutes and monovalent salts solutions [37]. Further development of the DSPM, i.e. the DSPM-DE, proposed by Vezzani and Bandini, consisted in the incorporation of the dielectric exclusion mechanism [41]. They showed that the prediction of rejections of divalent ions, such as Mg^{2+} and Ca^{2+}, significantly improves including this mechanism in the ionic partition.

Many works in the literature presented a characterization of NF membranes with different salt solutions, by performing ad hoc designed experiments coupled with DSPM-DE simulations. Most of the works focused on the characterization of commercial NF membranes in the presence of single salt solutions. Mohammad et al. investigated the impact of the solution concentration on the membrane charge density with NF90 membranes and six single salt solutions (NaCl, KCl, $MgCl_2$, Na_2SO_4, Na_2CO_3, $MgSO_4$) [42]. They found that the DSPM-DE can predict the water flux and the salt rejection also at high concentrations. Moreover, since dielectric exclusion and charge density are interconnected, in order to split the two effects, many authors focused on the identification of the isoelectric point, i.e. the pH at which the membrane charge is equal to zero. The identification of the isoelectric point allows first for estimating the dielectric constant and secondly for calculating the charge density, by fitting model simulations to rejection data. Following this procedure, Mazzoni et al. characterized Desal DK membranes with NaCl and $CaCl_2$ solutions [43] and Hussain et al. characterized two commercial membranes with NaCl solution and investigated how the membrane charge density is affected by different concentrations in the presence of NaCl and $MgCl_2$ solutions [44]. Kotrappanavar et al. reported membrane parameters for NF250 and NF300 with NaCl and $MgCl_2$ solutions at different concentrations, by using the Stokes-Einstein, Born effective and Pauli radii for the model simulations [45]. Oatley et al. focused on the identification of the isoelectric point with NaCl and KCl solutions and reported the dielectric constant within the pores found via model fitting for four different salt solutions with two membranes (NF270 and NF99HF) [3].

Only a few papers report a comprehensive characterization of membranes in the presence of multi-ionic solutions with experimental results and model fitting [4,46,47]. Roy et al. performed a fit of the DSPM-DE to experimental data to estimate the NF membrane parameters for seawater [48]. A study by Labban et al. reports the characterization of low-pressure hollow fibre membranes [49]. They identified the isoelectric point by varying the pH of a NaCl solution and they found the membrane charge density for three different mixtures via model fitting to rejection data: NaCl–$MgCl_2$; NaCl–Na_2SO_4 and artificial seawater.

Overall, the characterization of NF membrane is essential to predict the performances of the NF process in the presence of different solutions. Only a few studies have characterized NF membranes with multi-ionic mixtures, although these are much more common than the single salt solutions in industrial applications and nature. In addition, despite the large number of works on the assessment of NF performances for different industrial applications, very few focus on the investigation of the membrane parameters with industrial streams.

To fill this gap, we performed the characterization of commercial NF membranes in the presence of an artificial solution simulating the effluent produced by the regeneration of ion exchange resins employed

for water softening. The joint experimental and simulation campaign carried out with two commercial membranes, NF270 and TS80, allowed for estimating the membrane parameters (pore radius, membrane thickness, pore dielectric constant and charge density) with a water-salt mixture (hereby referred to as "brine") simulating the real wastewater effluent. Since the NF membrane properties strongly depend on the feed composition and concentration, performing a comprehensive characterization for the specific industrial application is very important. In fact, the results of the present work allow for predicting accurately the membrane behaviour in the industrial application and for designing bigger-scale NF plants, accounting for real membrane properties. Moreover, the same experimental campaign was performed with a ten-time diluted solution (hereby referred to as "diluted brine"), to assess the role of the concentration of the multi-ionic solutions on the membrane properties.

Overall, the analysis of the collected data with the two membranes and at two different concentrations gives insights into the exclusion and the trans-membrane transfer mechanisms that are responsible for the ionic rejections.

2. Theoretical background: the Donnan Steric Pore Model with Dielectric Exclusion

This section describes the theory about the transfer and exclusion mechanisms in NF membrane and reports the main equations of the Donnan Steric Pore Model with Dielectric Exclusion (DSPM-DE), which has been widely used in the literature to simulate NF membranes.

The DSPM-DE is based on the extended Nernst-Planck equation that defines the flux of ions through the membrane as the combination of three transport mechanisms, i.e. convection, diffusion, and electromigration [37]. Other fundamental equations are related to the equilibrium partition at the interfaces and the electro-neutrality condition. The partition of the ions at the solution-membrane interface depends on the ionic size (steric partition), the charge of the ions and of the membrane (Donnan partition) and the dielectric constant within the pores, that determines the solvation energy (dielectric partition) [50]. These exclusion mechanisms have been widely investigated in literature and many efforts have been dedicated to identifying the impact of the membrane parameters (pore radius, membrane thickness, pore dielectric constant and charge density) on the performance. In particular, many studies focused on the estimation of the pore dielectric constant and the charge density, which are responsible for the dielectric exclusion and the Donnan exclusion, respectively [47,51]. The dielectric exclusion is mostly caused by the different solvent structure in the narrow pores, which is responsible for the increase of the ion solvation energy within the pores. The charge density depends on various mechanisms that take place once the membrane comes in contact with an aqueous solution, such as the dissociation of the functional groups and the adsorption of ions from the solution onto the membrane [52]. Experimental evidence showed that the two parameters are dependent and that both are a function of the solution composition [43]. The dielectric constant of a membrane may significantly change when varying the feed composition: Oatley et al. found similar values of dielectric constant in the presence of solutions of NaCl, KCl and Na_2SO_4 (between 31 and 35 for Desal DK membrane and between 38 and 42 for NF270) and higher values with $MgSO_4$ solutions (46.6 for Desal DK membrane and 65.1 for NF270) [3,50]. Moreover, the ions present in the solution have a crucial role in the charge density: the ions can adsorb onto the membrane surface and can affect the charge significantly, depending on their concentration. For example, it was found that high concentrations of divalent cations may cause an increase of membrane charge, which can turn into positive, even in presence of negatively charged functional groups [52–54].

2.1. Mathematical formulation of the DSPM-DE

The extended Nernst-Planck equation, reported below (equation (1)), defines the flux of each ion through the membrane.

$$j_i = J_v C_i^p = -D_{i,pore}\frac{dC_i^m}{dy} - z_i C_i^m D_{i,pore}\frac{F}{RT}\frac{d\psi}{dy} + k_{i,c} C_i^m J_v \quad (1)$$

The flux j_i of each ion *i* through the membrane, which is equal to the product of the water flux J_v and the concentration of the ion *i* in the permeate solution C^p_i, is given by the sum of three terms. The first (diffusive flux) depends on the diffusion coefficient of the ion inside the pore ($D_{i,pore}$) and the concentration C^m_i change within the membrane itself (y-axis). The second (migrative flux) depends on the potential profile (ψ) along the membrane thickness, the diffusion coefficient of the ion inside the pore ($D_{i,pore}$), the ionic concentration C^m_i, the ion valence (z_i), the Faraday (F) and the ideal gas constants (R) and the temperature (T). Finally, the third (convective flux) is a function of the convective coefficient of the ions inside the pores ($k_{i,c}$), the water flux and the ionic concentration inside the membrane. Fig. 1 depicts the water and the ionic fluxes through the membrane and typical profiles of concentration and electric potential.

The water flux through the membrane can be expressed as a function of the net pressure difference ΔP, the pore radius r_p, the membrane thickness δ_m and the solution dynamic viscosity η, according to the Hagen-Poiseuille equation (equation (2)). The net pressure difference ΔP is given by the difference of the applied pressures in the feed-concentrate and in the permeate channel minus the osmotic pressure difference $\Delta\Pi$, as shown in equation (3).

$$J_v = \frac{\Delta P\, r_p^{\,2}}{8\,\eta\,\delta_m} \quad (2)$$

$$\Delta P = \left(P^f - P^p\right) - \Delta\Pi = \left(P^f - P^p\right) - RT\sum_i \left(C^{bm}{}_i - C^p{}_i\right) \quad (3)$$

The diffusion and the convective coefficients require a specific definition, given the size of the pores where these transports occur. Therefore, "hindered" or "restricted" transport can be described through the introduction of the hindrance factors for diffusion and for convection, $k_{i,d}$ and $k_{i,c}$ [55].

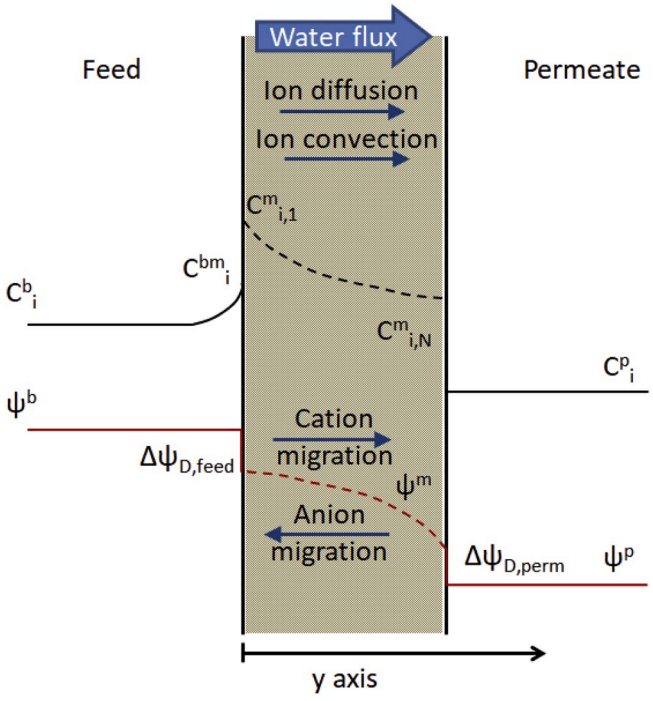

Fig. 1. Schematic of the NF membrane, including the indication of the ionic and water fluxes and exemplary ionic concentration and potential profiles.

$$D_{i,pore} = k_{i,d} D_{i,\infty} \tag{4}$$

$$k_{i,d} = \frac{1}{\varphi_i}\left(1 + \tfrac{9}{8}\,\lambda_i\, ln(\lambda_i) - 1.56034\,\lambda_i + 0.528155\,\lambda_i^2 + 1.91521\,\lambda_i^3 - 2.81903\,\lambda_i^4 + 0.270788\,\lambda_i^5 + 1.10115\,\lambda_i^6 - 0.435933\,\lambda_i^7\right) \tag{5}$$

$$k_{i,c} = \frac{1 + 3.867\,\lambda_i - 1.907\,\lambda_i{}^2 - 0.834\,\lambda_i{}^3}{1 + 1.867\,\lambda_i - 0.741\,\lambda_i{}^2} \tag{6}$$

The coefficients $k_{i,d}$ and $k_{i,c}$ are functions of the parameter λ_i, which is given by the ratio between the ion Stokes radius and the pore radius.

Concerning the solution-membrane interface, the equilibrium partition can be described by equation (7) for the feed-membrane interface and by equation (8) for the permeate-membrane interface.

$$\frac{\gamma^m{}_{i,1} C^m{}_{i,1}}{\gamma^{bm}{}_i C^{bm}{}_i} = \varphi_i \varphi_{Bi} \exp\left(-\frac{z_i F}{RT}\Delta\psi_{D,feed}\right) \tag{7}$$

$$\frac{\gamma^m{}_{i,N} C^m{}_{i,N}}{\gamma^p{}_i C^p{}_1} = \varphi_i \varphi_{Bi} \exp\left(-\frac{z_i F}{RT}\Delta\psi_{D,perm}\right) \tag{8}$$

In equation (7), the ratio between the activity of the ion just inside the membrane on the feed-concentrate side (index 1) and just outside the membrane in the feed solution (index bm) is proportional to the steric coefficient φ_i, the Born solvation coefficient φ_{Bi} and the Donnan term. The latter depends on the Donnan potential at the solution membrane interface $\Delta\psi_{D,feed}$ [56]. The same can be said for equation (8), where the ratio is between the activity of the ions just inside the membrane on the permeate side (index N) and the activity in the permeate solution. In the permeate solution, the concentration polarization is negligible, thus there is no need to define a concentration of the permeate solution just outside the membrane (as $C^{bm}{}_i$).

The activity coefficients are calculated via the Davies equations, given in equations (9) and (10) [57].

$$\log \gamma_i = -A\, z_i{}^2\left(\frac{\sqrt{I}}{1+\sqrt{I}} - 0.3\, I\right) \tag{9}$$

$$A = \frac{e_0{}^3\, N_A{}^{1/2}}{\ln(10)\, 4\pi\, \sqrt{2}\, (\varepsilon\, k_B T)^{3/2}} \tag{10}$$

The exclusion coefficients are calculated as below. The steric coefficient depends on the parameter λ_i, whereas the Born solvation coefficient depends on the solvation energy barrier, calculated using the Born model as a function of the dielectric constants in the pore (ε_{pore}) and in the solution bulk (ε_b) [58].

$$\varphi_i = (1 - \lambda_i)^2 \tag{11}$$

$$\varphi_{Bi} = \exp\left(-\frac{\Delta W_i}{k_B T}\right) \tag{12}$$

$$\Delta W_i = \frac{z_i{}^2 e_0{}^2}{8\pi\varepsilon_0 r_i}\left(\frac{1}{\varepsilon_{pore}} - \frac{1}{\varepsilon_b}\right) \tag{13}$$

The concentration at the feed membrane interface depends on the concentration polarization that consists in a concentration gradient between bulk and membrane interface. This gradient is due to the fact that the ions would have different rates in crossing the membrane and in moving from the bulk to the membrane. The concentration polarization leads typically to higher concentrations of the ions at the membrane interface that contribute to decreasing the permeate flux and the ionic rejections. This phenomenon can be quantified by equating the ion flux through the membrane to the one from the bulk to the membrane interface, as in equation (14) [59].

$$j_i = -k'^b_{c,i}\left(C^{bm}{}_i - C^b{}_i\right) + J_v C^{bm}{}_i - z_i C^{bm}{}_i D_{i,\infty}\frac{F}{RT}\xi \tag{14}$$

The mass transfer coefficient (equation (15)) is estimated using the equation given for spiral wound membranes by Senthilmurugan et al. and is corrected using the coefficient Ξ, which accounts for the "suction effect" due to the membrane permeation [60].

$$k'^b_{c,i} = k^b_{c,i}\,\Xi = k^b_{c,i}\left[\frac{J_v}{k^b_{c,i}} + \left(1 + 0.26\left(\frac{J_v}{k^b_{c,i}}\right)^{1.4}\right)^{-1.7}\right] \tag{15}$$

$$k^b_{c,i} = 0.753\left(\frac{\eta_{mix}}{2-\eta_{mix}}\right)^{1/2}\left(\frac{D_{i,\infty}}{h_f}\right) Sc^{-1/6}\left(\frac{Pe_i h_f}{L_{mix}}\right)^{1/2} \tag{16}$$

In equation (16), η_{mix} is the mixing efficiency of the net of the spacer, h_f is the height of the feed channel, L_{mix} is the mixing length of the spacer, Pe and Sc are the Peclet and the Schmidt adimensional numbers, respectively.

Furthermore, other conditions to be fulfilled are the electroneutrality at the feed-membrane interface, in the permeate solution and inside the membrane. These conditions are given in equations (17)–(19).

$$\sum_i z_i C^{bm}{}_i = 0 \tag{17}$$

$$\sum_i z_i C^p{}_i = 0 \tag{18}$$

$$\sum_i z_i C^m{}_{i,j} + X_d = 0 \tag{19}$$

The system of equations was solved following the implementation proposed by Geraldes et al. [61]. The equations were discretized within the membrane and linearized, by defining linear coefficients containing guess values of electric potential and ionic concentrations. The linear system of equations was solved simultaneously in Python via the *LAPACK routine_gesv*, then the coefficients of the linear system were recalculated and the updated system was solved again. The iterative procedure was repeated until all conditions were fulfilled and the residuals were below 10^{-4} [61].

3. Materials and methods: experiments for membrane characterization

This section focuses on the description of the experimental activities performed for characterization purposes. The experiments are schematically reported in Table 1.

Membrane filtration experiments were carried out in a laboratory-scale flat sheet cross-flow SEPA-CFII cell by Osmonics, depicted in Fig. 2. The membrane, with an active area of 0.014 m^2, was placed into the membrane housing that was kept pressurized during the experiments. The module contained a piston feed pump, pressure indicators on the feed and the concentrate side, and a regulation needle valve for the concentrate stream, which was manually controlled to adjust the transmembrane pressure. The permeate and the concentrate flows were measured by mass flowmeters (Mini Cori-Flow and Gems Sensors, respectively). Two different NF membranes were tested in this study: (i) NF270 (DOW Filmtec, USA) and (ii) TS80 (Trisep Microdyn Nadir, Germany). NF270 has been widely used in the literature and in industrial applications for the removal of divalent ions. Therefore, it has been chosen as a reference membrane, because the availability of published data relevant to NF270 membrane allowed for assessing the validity of our experimental methods [62]. Conversely, TS80 is much less common and, from a preliminary comparison of various membranes, it resulted particularly suitable to divalent cations separation. Both membranes are made of a thin polyamide active layer and a polysulfone support layer but they belong to different categories in terms of membrane chemistry. NF270 is a semi-aromatic membrane (PIP-TMC), whereas TS80 (MPD-TMC) is a fully aromatic membrane. The membranes were wetted

Table 1
Experimental activities performed in the present work.

Experiment	Operating solution	Variable input	Measured output	Membrane parameter to estimate
Permeability test (Sections 3.1, 4.1)	Pure water	Trans-membrane pressure	Permeate flux	Pore radius and active layer membrane thickness
Organics rejection (Sections 3.1, 4.1)	Solutions of organics	Trans-membrane pressure	Permeate concentration	
Ionic rejection varying pH (Sections 3.2, 4.2)	Feed solution (brine and diluted brine)	Solution pH	Permeate concentration	Pore dielectric constant and charge density
Ionic rejection varying permeate flux (Sections 3.3, 4.3)	Feed solution (brine and diluted brine)	Permeate flux	Permeate concentration	

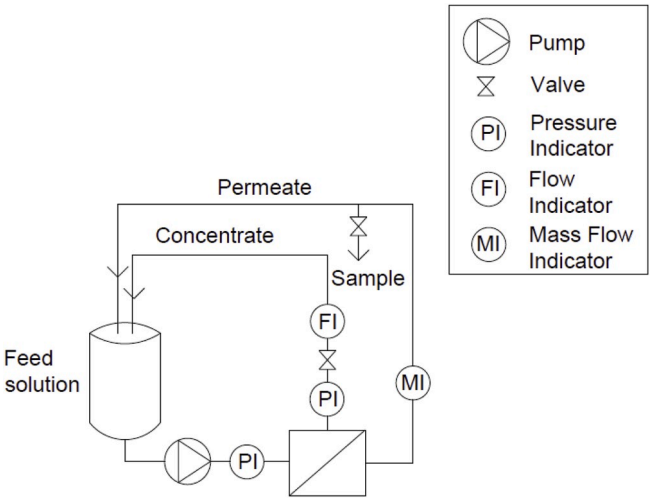

Fig. 2. Scheme of the laboratory-scale flat sheet cross-flow cell SEPA-CFII by Osmonics, used for the experiments.

and kept immersed in demineralized water for 24 h prior to each experiment. The feed water temperature was monitored by a thermometer and remained constant at 21 °C during the experiments through a cooling spiral that was immersed in the feed tank. Before each experiment, the membrane was pressurized for 2 h at a constant flux and the permeate and the concentrate streams were mixed with the feed solution. After this stabilization period, the solutions were circulated and samples were collected after 30 min and 1 h. The cross-flow velocity was 1 m/s, in order to diminish the effect of concentration polarization and to ensure the equality between observed and real ion rejections. The ion rejection was calculated using equation (20) and the experiments were repeated twice to validate the data.

$$R_i = 1 - \frac{C^p{}_i}{C^f{}_i} \tag{20}$$

3.1. Permeability test and organics rejection

Permeability test and organics rejection measurement are fundamental to evaluate membrane pore radius and active layer membrane thickness, which are closely related.

3.1.1. Procedure to estimate the pore radius

The calculation of the pore radius of the two membranes was performed by testing three neutral solutes (glycerol, glucose and sucrose) as it was proposed by Bowen et al. and then applied by many authors [37, 63]. Low concentrations of the neutral solutes (200 mg/l) and relatively high cross-flow velocity (1 m/s) were used to minimize the effect of concentration polarization and the difference between the observed and the real rejections. Four different permeate fluxes were tested and used for model calibration: 35, 70, 105 and 170 L/(m^{2}h). The experimental rejection of the single organic solutions was calculated from Total Organic Carbon (TOC) analysis of the permeate and the feed samples by using the TOC-V_{CPH} analyser and the ASI-V autosampler (Shimadzu, Japan).

The trans-membrane flux of the neutral solutes is based only on diffusion and convection and their theoretical rejection is due to steric interactions with the pore wall. The values of organics rejection were calculated as functions of the pore radius, according to equation (21) [50]. Thus, the pore radius of the membrane was calculated by minimizing the sum of squared errors (SSE) between the calculated and the experimental ionic rejections, as reported in equation (23). Then, an average pore radius based on the fitting values found for the three employed neutral solutes (i.e. glycerol, glucose and sucrose) was estimated. The physical properties of the three organics are summarized in Table 2.

$$R_i = 1 - \frac{C^p{}_i}{C^f{}_{i,w}} = 1 - \frac{k_{i,c}\varphi_i}{1 - [1 - k_{i,c}\varphi_i]\exp(-Pe_i)} \tag{21}$$

$$Pe_i = \frac{k_{i,c}J_v\delta_m}{D_{i,p}} = \frac{k_{i,c}r_p{}^2}{8\eta D_{i,p}}\Delta P \tag{22}$$

$$SSE = \sum_i \left(R_{i,exp} - R_{i,calc}\right)^2 \tag{23}$$

The neutral solute rejection increases when the applied pressure increases because convection becomes the primary transport mechanism and the permeate stream is less concentrated. A plateau is reached when any further increase in the applied pressure does not contribute to an increase in the uncharged solute rejection. In fact, the rejection remains constant because the effect of higher convective fluxes is counterbalanced by an increase of concentration polarization and, consequently, of the solute transport to the permeate side [49]. This rejection, namely the limiting rejection (R_{lim}), is defined in equation (24) and it is obtained when the Peclet number (Pe) reaches very high values.

$$R_{i,lim} = 1 - k_{i,c}\varphi_i \tag{24}$$

In this study, high permeate fluxes were tested in order to reach the

Table 2
Properties of the neutral solutes and the ions used for the experiments [49].

Solute	MW (g/mol)	r_i (nm)	$D_{i,oo}$ (x 10^{-9} m^2 s^{-1})
Glycerol	92	0.260	0.95
Glucose	180	0.365	0.69
Sucrose	342	0.471	0.52
Na^+	23	0.184	1.33
Cl^-	35	0.121	2.03
Mg^{2+}	24	0.347	0.706
Ca^{2+}	40	0.309	0.792

limiting rejection of the solutes.

3.1.2. Procedure to estimate the active layer membrane thickness

The active layer membrane thickness (δ_m) is defined as the ratio between the effective thickness and the porosity [37] and it is calculated via membrane permeability experiments once the pore radius is known. In this study, the membrane permeability was measured by filtering demineralized water at different transmembrane pressures and by monitoring the permeate flux. A linear trend between the applied pressure and the permeate flux was observed in membrane filtration experiments [44]. The effective membrane thickness was calculated by the Hagen-Poiseuille equation (see equation (2) in section 2) and by assuming that the pore radius of the membrane is cylindrical and uniform [49].

3.2. Ionic rejection varying pH

To assess the behaviour of the membranes in the presence of salt mixtures, we measured the ionic rejections at different values of feed solution pH.

For these experiments, a brine given by the mixture of three salts (NaCl, $CaCl_2{\cdot}2H_2O$, and $MgCl_2{\cdot}6H_2O$), simulating the real wastewater produced by the ion exchange columns, was used as feed solution. Additional experiments were conducted to investigate the influence of the ionic strength on the exclusion effects, by diluting the artificial brine ten times. The properties of the ions (Stokes radius and bulk diffusivity) are reported in Table 2 and the concentrations of the brine and the diluted brine are reported in Table 3. The pH of the feed solution was varied between 3 and 9 with the addition of NaOH and HCl and it was measured using a multi-parameter portable meter (Multi 3510 IDS) with a WTW pH electrode. Permeate fluxes of 15, 30 and 45 L/(m^2h) were tested for each membrane (TS80 and NF270), solution (brine and diluted brine) and pH. Samples were taken after the stabilization period, and the electrical conductivity was measured with a WTW EC probe to check the stability of the permeate water quality and the representativeness of the sample. The samples were analysed by Inductively Coupled Plasma Mass Spectrometry (ICP-MS) and by Inductively Coupled Plasma - Optical Emission Spectrometry (ICP-OES).

3.3. Ionic rejection varying permeate flux: estimation of pore dielectric constant and membrane charge density

For the estimation of the pore dielectric constant and the charge density of each membrane, a curve fitting was performed by minimizing the sum of squared errors (SSE) between the measured and the calculated rejection of the feed solution (defined in equation (25)).

$$f_{obj}(\varepsilon_{pore},\ X_d) = SSE = \sum_{fluxes}\sum_{i}\left(R_{i,exp} - R_{i,calc}\right)^2 \tag{25}$$

For this analysis, membrane experiments were conducted at four fluxes (15, 30, 45 and 70 L/(m^2h)) and by using the salt mixtures of Table 3. The sampling and ion analysis procedures were the same as described in section 3.2.

The range of fluxes was selected in order to cover a wide range of operating conditions and in particular pressures since these fluxes correspond to feed pressures from 1 to 32 bar. Although typical fluxes for long-run operations with wastewater do not exceed 25 L/(m^2h) [64], we performed experiments also at higher fluxes to obtain a broader set of data for model calibration.

In literature, the estimation of the pore dielectric constant has been often performed via the least-square fitting of the ionic rejections at the isoelectric point, i.e. the pH at which the rejection reaches a minimum because the charge density equals zero and the steric and the dielectric effects are the only exclusion mechanisms. In the presence of multi-component systems, the isoelectric point often corresponds to the pH range where a net variation of the ionic rejection trends occurs, because this is likely due to a switch in the membrane charge [62].

In the present work, we also implemented this second method, to confirm the findings of the first method. The pore dielectric constant was assessed by minimizing the error between the ionic rejections calculated by fixing the charge density to zero and the values measured at the pH range corresponding to a net variation of the trend. Once the pore dielectric constant was known, the membrane charge density was estimated by minimizing the error between the calculated and the measured ionic rejections in the presence of the feed solution.

Table 3
Concentrations of the artificial brine and the diluted brine.

Solute	Ion concentration (ppm)		Ion concentration (mol/m^3)	
	Brine	Diluted brine	Brine	Diluted brine
Sodium	4030	403	175	17.5
Calcium	7640	764	191	19.1
Magnesium	1260	126	52.5	5.25
Chloride	23,200	2320	662	66.2

4. Results and discussion

In this section, the results of the experimental and simulation campaigns are reported, with the aim to present a full characterization of two commercial NF membranes with a salt mixture (brine) analogous to the wastewater produced by ion exchange resins. Firstly, we show the results of the permeability tests together with the values of rejections found for organic solutes, which allow for estimating the pore radius and the active layer membrane thickness. Secondly, we present the experimental values of rejection of the different ions when the solution pH is varied, to assess how the ionic rejections are affected by the pH and, consequently, by the membrane charge density. Thirdly, we report the ionic rejections at different permeate fluxes, which we used to calculate the pore dielectric constant and membrane charge density, through a least-square fitting of the model to the experimental results.

4.1. Permeability test and organics rejection: estimation of pore radius and active layer membrane thickness

The results of the permeability test for NF270 and TS80 are depicted in Fig. 3. A linear relationship between water flux and applied pressure was found, as expected, and the slope, corresponding to the membrane

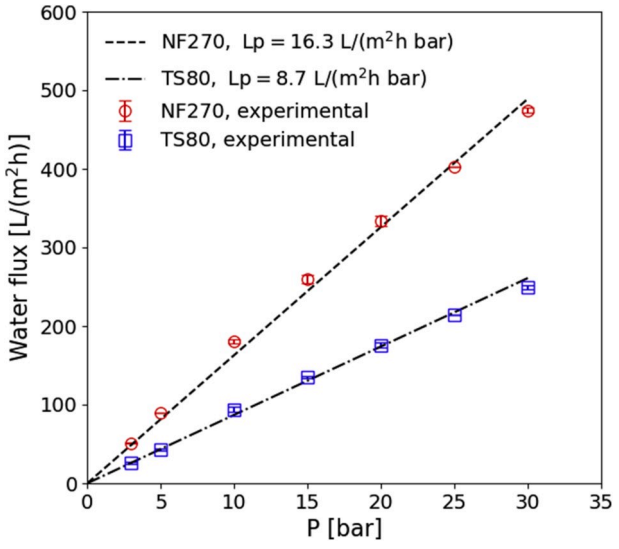

Fig. 3. Experimental water flux through the membrane [L/(m^2h)] vs. the applied pressure [bar] for NF270 and TS80.

permeability, resulted equal to 16.3 L/(m^2h)/bar for NF270 and 8.7 L/(m^2h)/bar for TS80. The two membranes showed very different values of permeability, which suggested that the steric exclusion mechanism was more effective in TS80 and this might lead to higher solute rejections.

The rejection values found for glycerol, glucose, and sucrose with NF270 and TS80 are depicted in Fig. 4. Solutes with lower Stokes radius showed lower rejection with both membranes. Moreover, the rejection of glucose and sucrose became constant already at low pressure, meaning that these solutes reached the limiting rejection. Conversely, almost constant rejection of glycerol was observed only with TS80 at the highest investigated pressures. Regarding the fitting of the theoretical curves to the experimental data, different pore radii were found for the different solutes and the lower the solute radius, the lower the fitting pore radius. This finding was already reported by previous authors, who found that the solutes experience different pore sizes and different membrane thicknesses depending on their size because the network of pores is more complex and tortuous than how it is usually represented [65]. In particular, smaller solutes such as glycerol have longer paths within the membrane and are able to detect smaller pore radii [66]. Therefore, to obtain a uniform pore size, the pore radius was estimated for each membrane as the average of the radii found with the different solutes [67]. In this way, we found a pore radius of 0.507 nm for NF270 and 0.488 nm for TS80. The pore radius of NF270 is in agreement with other studies in literature, which report values in the range of 0.43–0.54 nm [3,67,68]. As already predicted by the permeability test, the NF270 membrane showed a larger pore radius than the TS80 and this was already highlighted by Wadekar et al., who found that semi-aromatic membranes as NF270 show larger effective pore sizes in comparison with fully aromatic membranes as TS80 [54]. The pore radii were slightly higher than the sucrose radius, whose rejection was equal to or higher than 90% in both membranes. Similarly, Labban et al. found rejection values of sucrose of 93% and a pore radius of 0.5 nm [49].

To assess the validity of assuming an average pore radius for each membrane, Fig. 5 shows the comparison between the experimental limiting rejection values and the theoretical curve, defined in equation (24). Since glycerol did not reach the limiting rejection within the investigated pressure range, the value of limiting rejection used in Fig. 5 corresponds to the plateau reported in Fig. 4. A good agreement was found for both membranes between theoretical and experimental values, with errors lower than 11%. Therefore, we can conclude that the membranes could be reliably modelled, assuming the aforementioned average pore radii.

Once the pore radius and the permeability (Fig. 3) were assessed for each membrane, the active layer membrane thickness was estimated, using the Hagen-Poiseuille equation (equation (2)). The membrane thickness obtained was equal to 0.8 μm for NF270 and 1.38 μm for TS80.

4.2. Ionic rejections varying the solution pH

To assess the membrane behaviour with the brine and the diluted brine and to estimate the other two membrane parameters (pore dielectric constant and membrane charge density), we measured the ionic rejections at different solution pH values and permeate fluxes. The data collected at different pH values are depicted in Fig. 6.

Firstly, the ions showed different values of rejections and, in particular, the order of rejection, in any case, was $R_{Mg} > R_{Ca} > R_{Cl} > R_{Na}$. This is because NF membranes are able to selectively separate ions on the basis of their Stokes radius, diffusivity, and valence. In all cases, the rejection rate of divalent ions was higher, as predicted by the values of Stokes radius and diffusivity reported in Table 2. Moreover, the rejections found with TS80 are higher than the ones with NF270 and this is in agreement with the lower pore radius and higher active layer membrane thickness found in section 4.1. A negative rejection of Na^+ was observed in the case of NF270 membrane, whereas positive values were found with TS80. In the first case, the higher transmembrane flux of Cl^- led to higher fluxes of the most mobile cation, i.e. Na^+, which had to compensate for the negative charge on the permeate side, since the divalent ions were more screened by the membrane [49].

Secondly, relatively flat trends of ionic rejections vs. the pH were found with both brine and diluted brine and for both membranes. Therefore, even if the membrane charge density changed with pH, the system did not seem to be significantly affected by these variations. In general, this finding suggests that, at the investigated concentrations, the Donnan exclusion mechanism does not give a significant contribution to the ionic rejection. This is in line with other studies that reported a flat membrane potential for solutions with ionic strengths higher than 0.1 M [4,54]. However, the semi-aromatic membrane (NF270) showed a more enhanced variation with pH in comparison with the fully aromatic membrane (TS80). In particular, while the rejections of Ca^{2+} and Mg^{2+} were almost constant with the TS80 membrane, they were more sensitive to pH variation with NF270. This can be explained because semi-aromatic membranes present more fixed charges on their surface in comparison with multi-aromatic membranes, thus they may be more affected by the Donnan potential [54]. Note that NF270 showed a significant change in the ionic rejection when the pH was between 4 and 5, while the profiles of ionic rejection with TS80, especially the Na^+ rejection, changed their slope for pH values between 5 and 6. In particular, with NF270, Ca^{2+} reported a more evident decrease in rejection when the pH increased, whereas Mg^{2+} was more stable. In fact, Mg^{2+} has a higher Stokes radius and can be more screened by the steric effect. Conversely, Ca^{2+} can be more influenced by the Donnan exclusion, especially at lower pH values, since the membrane is more positively charged [52]. For pH higher than 5 for NF270 and higher than 6 for TS80, the ionic rejections were almost constant. Furthermore, the lower ionic rejections found with NF270 at the highest investigated pH

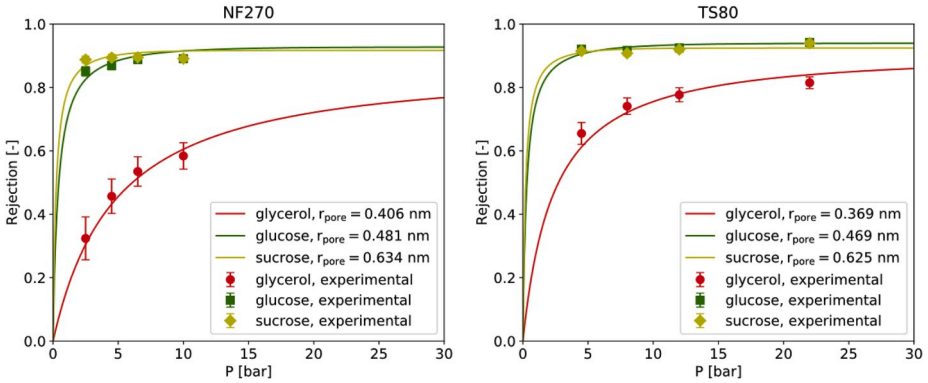

Fig. 4. Experimental rejections of neutral solutes at different applied pressures and model fitting curves at different pore radius for NF270 membrane (left) and TS80 membrane (right).

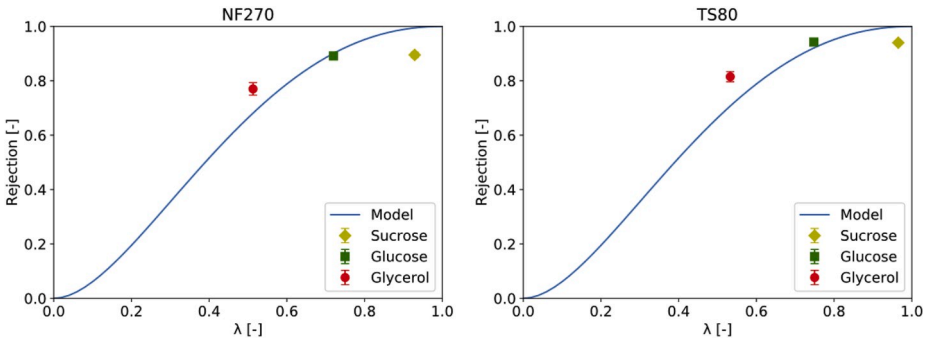

Fig. 5. Experimental values of limiting rejection of the three neutral solutes vs. the lambda ratio (solute Stokes radius divided by the pore radius) and the theoretical curve of limiting rejection vs. the lambda ratio for NF270 (left) and for TS80 (right).

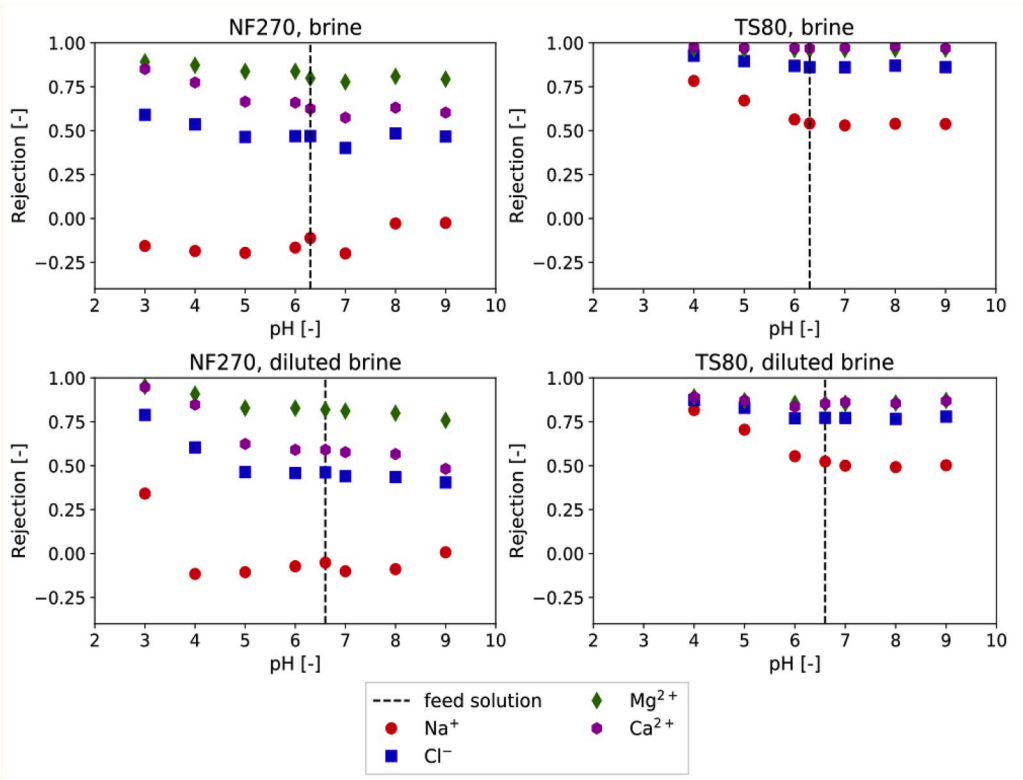

Fig. 6. Experimental rejection of each ion vs. the pH with NF270 and TS80 membranes and with the brine and the diluted brine, reported in Table 3. Flux = 45 L/(m^{2}h).

(i.e. 9) can be explained by considering the change of membrane morphology, because the pore radius tends to increase with alkaline solutions [68]. Overall, the trends of the ionic rejection vs. the solution pH gave essential insights into the transport mechanisms through the membrane at different operating conditions but did not allow for identifying a pH corresponding to a minimum rejection for every ion.

4.3. Ionic rejection varying permeate flux: estimation of pore dielectric constant and membrane charge density

To identify the pore dielectric constant and the charge density of the two membranes, firstly, we carried out experiments to measure the ionic rejections in presence of the synthetic wastewater (brine) and the diluted brine at four permeate fluxes (15, 30, 45 and 70 L/(m^{2}h)), corresponding to four different applied pressures (in the range between 1 and 32 bar). Secondly, we found the set of pore dielectric constant and membrane charge density by minimizing the SSE calculated as in equation (25) in Section 3.4.

The impact of the simultaneous variation of pore dielectric constant and membrane charge density on the SSE is reported in the maps in Fig. 7. The maps show that the charge density influences only slightly the systems at higher concentrations (brine) since the variation of the SSE is almost completely due to the change in the pore dielectric constant. Conversely, the maps relevant to the diluted brine present significant variations in both directions. This difference is explicable considering that the higher the ionic strength of the solution, the flatter the membrane potential and the lower the system dependence on the Donnan exclusion mechanism. However, it is worth noting that both maps for TS80 show a good fitting (low SSE) along an entire line of charge density vs. dielectric constant. This evidence, in line with the trends depicted in Fig. 6, demonstrates that the performances of the TS80 membrane are always governed by the dielectric constant, rather than the charge density.

From the minimization of the SSE, we identified the couples (ε_{pore},

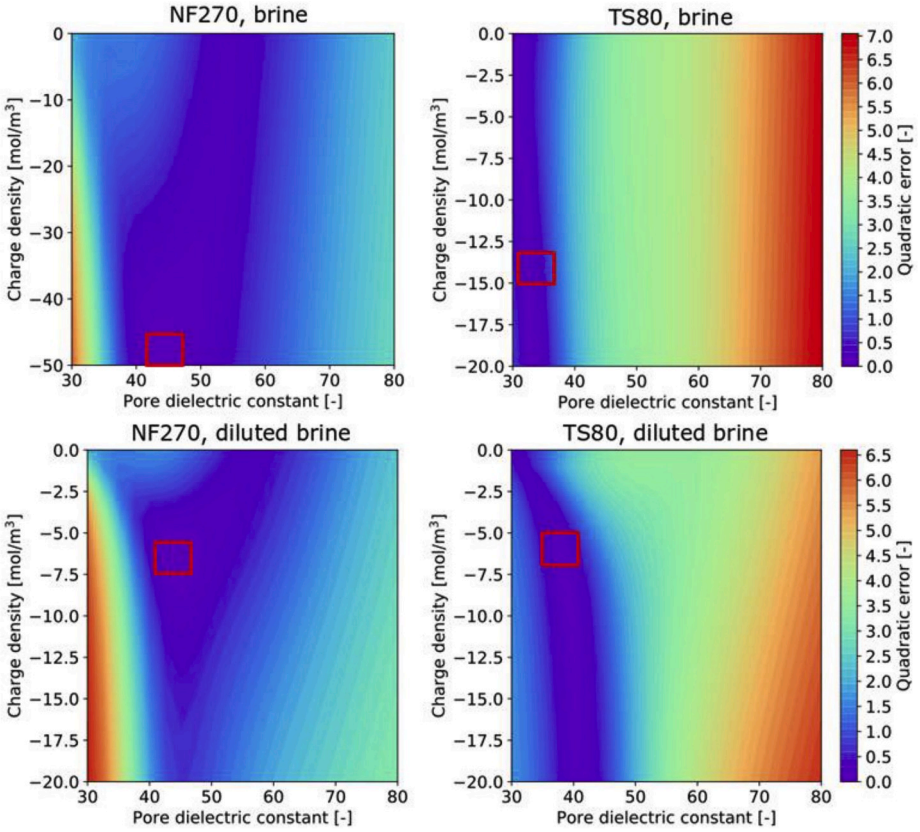

Fig. 7. Maps reporting the quadratic error (SSE) between the experimental and the calculated feed rejection values varying the pore dielectric constant and the charge density with brine and diluted brine and with NF270 and TS80 membranes. The red squares represent the minimum errors. (For interpretation of the references to colour in this figure legend, the reader is referred to the Web version of this article.)

X_d) able to describe the membrane behaviour with the minimum error. The estimated values of the membrane parameters, highlighted with the red squares in Fig. 7, are reported in Table 4. The results show that NF270 presented a higher ε_{pore} and a lower (more negative) X_d. Both findings justify the lower ionic rejections found with NF270, as reported in Fig. 6. Moreover, both membranes presented a higher ε_{pore} and a higher (less negative) X_d in the presence of the diluted brine. The lower dielectric constant at higher concentrations is due to the higher confinement of water within the pores when more ions are present. In fact, the dielectric exclusion is typically more effective in the presence of more concentrated solutions. Concerning the charge density, since Cl^- had a much higher concentration in comparison with the divalent ions, its adsorption had likely the greatest influence on the membrane charge density. In fact, the brine presented higher amounts of Cl^-, whose adsorption led to more negative charges. This is in line with the charge density found by Deon et al. who varied the concentration of NaCl and $CaCl_2$ [69].

Furthermore, we applied an additional method to identify one of the two parameters of the couple (ε_{pore}, X_d) of each membrane, to validate the results of the minimization algorithm, since the minimum was not always easily distinguishable, as shown in the maps of Fig. 7.

Table 4
Values of pore dielectric constant (ε_{pore}) and membrane charge density (X_d) estimated in the presence of the artificial brine and the diluted one with NF270 and TS80 membranes.

Membrane	Brine		Diluted brine	
	ε_{pore} [−]	X_d [mol/m^3]	ε_{pore} [−]	X_d [mol/m^3]
NF270	42.5	−50	45	−7
TS80	32.5	−14	37.5	−6

Such method consisted in estimating the pore dielectric constant by fitting the model trends to the ionic rejections found at the pH range corresponding to the isoelectric point. This was identified, in agreement with previous studies, by assuming that a change in the trends of the ionic rejection is attributed to a switch of the membrane charge sign [62]. Therefore, to assess the validity of the results reported in Table 4, the ionic rejections found between a pH of 4 and 5 for NF270 and between 5 and 6 for TS80 were used to recalculate the pore dielectric constant, assuming a charge density of zero. The least-square fitting gave values of pore dielectric constant between 45 and 50 for NF270 and between 30 and 35 for TS80. These values are in line with those found via the minimization algorithm (reported in Table 4) and fall within the range of previous results reported in the literature for seawater or solutions containing divalent ions [3,4,49,70]. Therefore, the application of an additional method for the estimation of pore dielectric constant and the comparison with results from the literature allow for validating the minimization method. Thus, the parameters obtained via such a method can be considered robust and reliable for model calibration.

Once the set of membrane parameters was found for each of the four membrane-solution combinations, simulations of the DSPM-DE were performed to compare the trends of the ionic rejections predicted by the model with all the collected experimental data. The results are depicted in Fig. 8. Note that the lowest permeate flux considered for the NF270 membrane with the diluted brine was 22 L/(m^{2}h) because lower pressure differences could not be imposed to reach lower fluxes. The error bars reported for the experimental points correspond to a 10% error in the permeate concentration, due to the precision of the instrument used for the concentration measurement. A good agreement between the trends given by the model and the experimental data was found: the errors were lower than 15% and the predicted values were within the error bars of the experimental values in almost all cases. Therefore, we

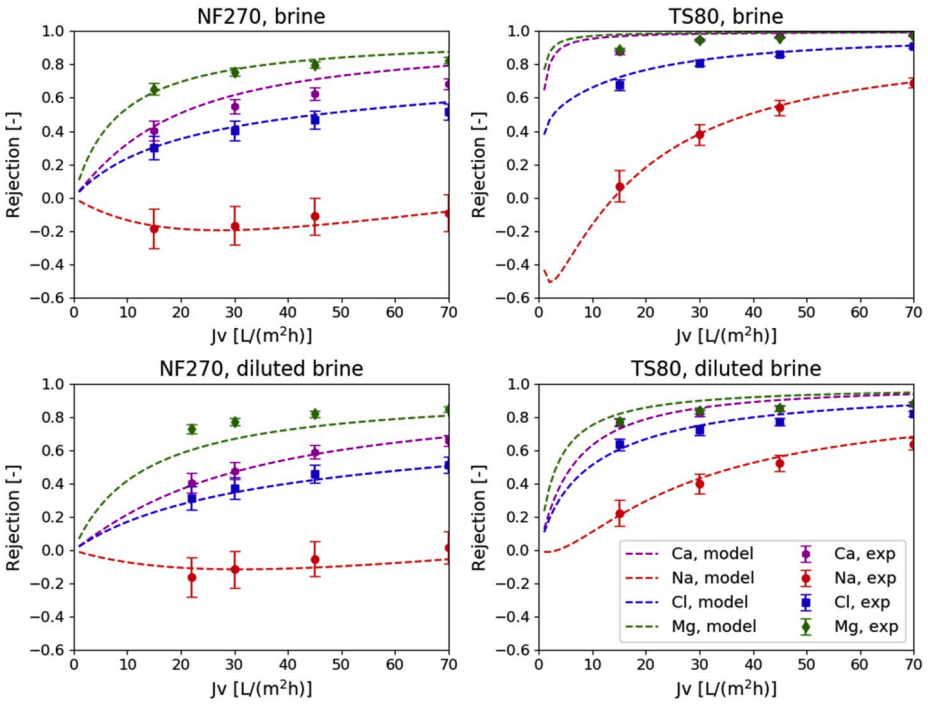

Fig. 8. Simulated trends of ionic rejection vs. the water flux Jv [L/(m^{2}h)] (dotted line) and experimental values of rejection at four fluxes (15, 30, 45 and 70 L/(m^{2}h)) obtained with brine and with diluted brine and for NF270 and TS80 membranes.

can conclude that the DSPM-DE was able to predict the performances of the NF membranes reliably in the presence of wastewater solutions, using the novel sets of four membrane parameters presented in this work.

5. Model results and discussion

Finally, an analysis of the ionic transmembrane fluxes estimated by the model was performed to get insights into the main transport and exclusion mechanisms occurring in the investigated systems. In particular, experimental rejections of the divalent ions at different feed concentrations and with the two membranes were compared and put in relation with the trans-membrane fluxes and the exclusion coefficients estimated by the model. The ionic rejections vs. the permeate flux are shown in Fig. 9. Firstly, in all cases, the rejections of the divalent ions increased with the flux since more water was forced to pass through the membrane and this led to a higher dilution of the permeate stream and a lower permeate concentration. Secondly, we found always higher rejections in the presence of the brine if compared with the diluted brine, except for Mg^{2+} that showed similar values of rejection at the two concentrations in the presence of NF270 membranes. Thus, the main experimental evidence concerns the decrease of rejections in the presence of diluted feed solutions and the stronger variation of rejection with TS80 membranes than with NF270.

The decrease in rejection at lower concentrations has been observed in literature for the case of solutions containing divalent cations. As a matter of fact, while with NaCl solutions the rejection increases when the concentration decreases, an opposite behaviour is observed with solutions of $MgCl_2$ or mixtures containing Mg^{2+} ions [44,46,71]. In these works, it was stated that the decrease of rejection with the concentration is due to the partial screening of the negative membrane charge caused by the adsorption of divalent cations, which occurs more at higher concentrations.

Our results are in line with those findings and in particular, the reduction of rejection is due to the fact that the concentration of the permeate solution decreased less than proportionally with the concentration of the feed. In fact, while the ratio between the feed concentrations in the brine and in the diluted brine was 10:1, the one between the experimental permeate concentrations was 12:1 for NF270 and 50:1 for TS80 (for a permeate flux of 45 L/(m^{2}h)).

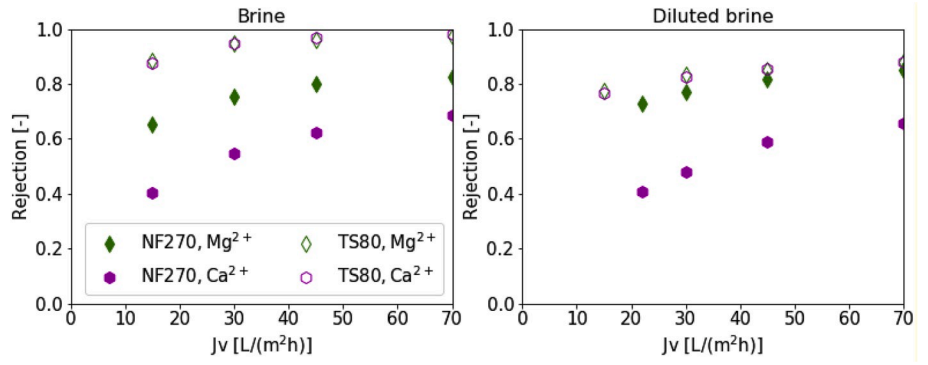

Fig. 9. Experimental ionic rejections for Mg^{2+} and Ca^{2+} vs. the permeate flux with the two membranes (NF270 and TS80) and the two feed solutions (synthetic brine and diluted brine).

This can be explained by analysing the transmembrane fluxes that are calculated by the model. The fluxes of Mg^{2+} and Ca^{2+} estimated for NF270 and TS80 membranes, with the two feed concentrations and a permeate flux of 45 L/(m^2h) are depicted in Fig. 10. The charts show the three contributions to the total ion fluxes. The total fluxes were related to the feed concentration but they did not decrease proportionally with the concentration: this led to a lower rejection with diluted feed solutions. Furthermore, the reduction of the total ionic fluxes was more enhanced with NF270 than with TS80 and this is in line with the stronger decrease of the ionic rejections with concentration found for TS80.

Concerning the analysis of the different fluxes, the diffusive flux was the highest term, and it decreased with the feed concentration because of the lower driving force, i.e. the concentration difference. Moreover, the migrative flux was lower for diluted brine because the potential profile within the membrane became flatter than the one with the brine. This variation was due to the decrease in the magnitude of membrane charge density, and consequently of the membrane potential difference, with the feed concentration, as already found in the literature [72]. Conversely, the convective flux with the diluted brine turned out to be slightly higher than the one with brine, in the presence of TS80 membranes. The concentration of ions in the membrane, as calculated by the model, was higher when a diluted feed solution was used. This effect can be explained by analysing the exclusion mechanisms at different feed concentrations.

The coefficients used to define the steric (φ_i), dielectric (φ_{Bi}) and Donnan (depending on $\Delta\psi_{D,bm}$) exclusion mechanisms for Mg^{2+} and Ca^{2+} are reported in Fig. 11, for the two membranes and the two feed solutions investigated. Firstly, the higher the exclusion coefficient, the lower was the impact of the corresponding exclusion mechanism. In all cases, the exclusion coefficients found for NF270 were higher than those found for TS80, which is in line with the higher rejections measured with TS80. Only the Donnan exclusion coefficients of the two membranes at high feed concentration were comparable since the charge density did not play a significant role in any case. At both concentrations and with both membranes, the steric coefficient was the largest term, meaning that the steric effect was always the least important one.

Conversely, the dielectric exclusion was the primary factor, in line with other studies showing how crucial the addition of the dielectric exclusion effect is to improve the model reliability in the presence of divalent ions [41]. The dielectric exclusion coefficient decreased at higher concentrations because the water was more confined within the pores, and the Donnan exclusion coefficient increased because the charge density effect was more screened. These findings are in agreement with previous works, reporting that the Donnan effect is more relevant at low feed concentrations and the dielectric effect at high feed concentrations [73,74].

Concerning the TS80 membrane, the dielectric exclusion mechanism had the highest impact and the increase of the relevant coefficient at lower feed concentrations led to an increase of the ionic concentration within the membrane (C^m). This caused higher convective fluxes of Mg^{2+} and Ca^{2+} through the membrane in comparison to the ones with brine. The increase in the convective flux was also responsible for the minor decrease of permeate concentration for TS80 (stronger reduction of rejection) when switching from the brine to the diluted brine if compared to the one found for NF270.

The analysis of the transmembrane ionic fluxes was also performed at a lower permeate flux (25 L/(m^2h)), to simulate operating conditions more similar to real NF units treating industrial wastewater. We found that the three fluxes and the three exclusion coefficients followed the same order for both bivalent ions and membranes: the diffusive was always the highest flux and the dielectric was always the primary exclusion mechanism. However, as expected, the convective flux was significantly lower because of the lower permeate flux driving it.

Overall, the analysis of the transmembrane fluxes and the exclusion mechanisms estimated by the model allowed highlighting the significant factors influencing the ionic rejections at different feed concentrations and with different membranes.

As mentioned in the introduction, to simulate the NF membranes reliably, it is crucial to characterize them by calibrating the membrane properties with the specific solution. In fact, among the available literature studies about the characterization of NF membranes, most works presented experiments performed with seawater or with peculiar solutions containing mixtures of magnesium and sodium chloride, whereas

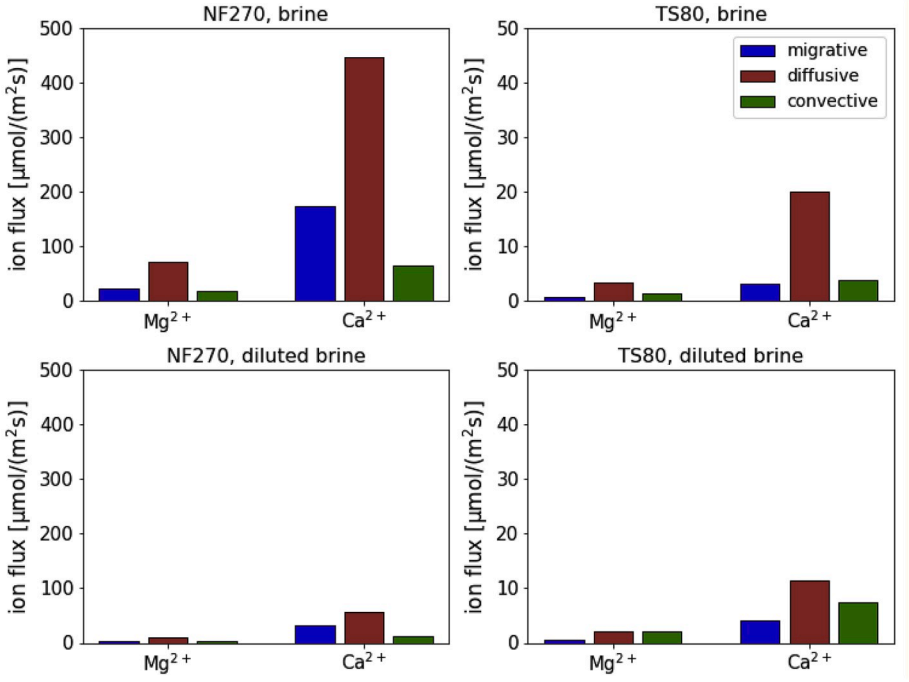

Fig. 10. Trans-membrane fluxes of Mg^{2+} and Ca^{2+} with NF270 and TS80 membranes, in the presence of synthetic brine and diluted brine. The permeate flux was 45 L/(m^2h).

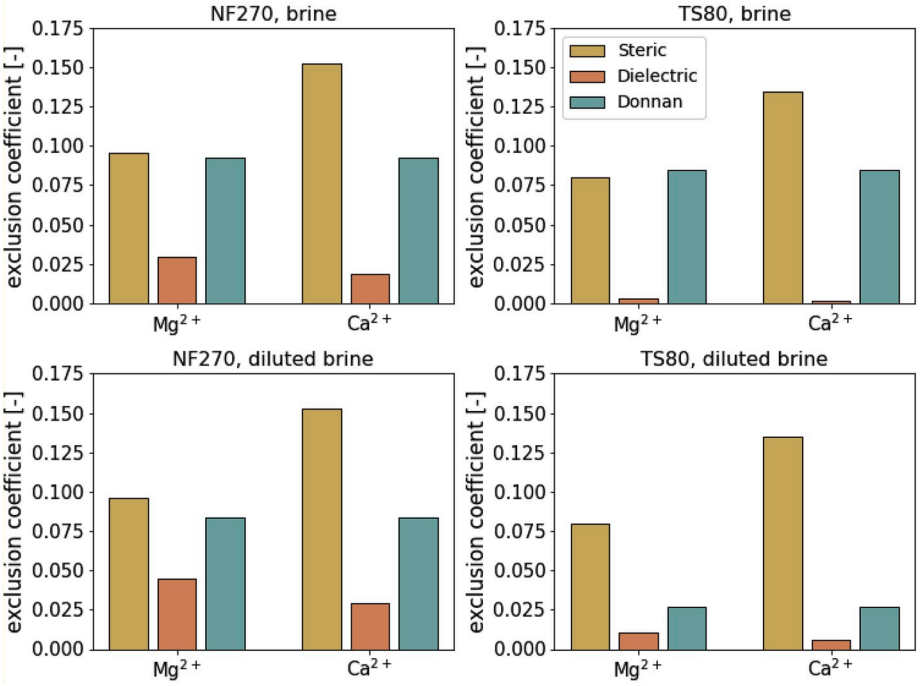

Fig. 11. Exclusion coefficients of Mg^{2+} and Ca^{2+} with NF270 and TS80 membranes, in presence of brine and diluted brine. The permeate flux was 45 L/(m^2h).

there are no studies about the characterization of NF membranes with the brines produced by ion exchange columns used in water softening.

With this respect, we run the DSPM-DE adopting our set of parameters of NF270 and other two found in the literature. In particular, we considered the membrane parameters found by Roy et al. for NF270 membrane and seawater [48] and the ones found by Labban et al. for hollow fibre membranes and seawater [49]. In all simulations, the feed solution of the NF unit corresponded to the spent regenerant of ion exchange resins used for water softening. The calculated rejection values for the different cases are shown in Fig. 12. We found that the two sets of parameters obtained for seawater were not suitable to simulate the NF membrane with our feed solution, characterized by higher ionic strength and relatively high concentrations of divalent ions. This analysis showed how much feed-dependant are the NF membrane parameters adopted in the model. Therefore, the joint experimental and simulation campaign is particularly important, since the knowledge of the suitable set of parameters allows for modelling the NF membranes reliably and for designing bigger-scale NF plant to purify the wastewater and implement

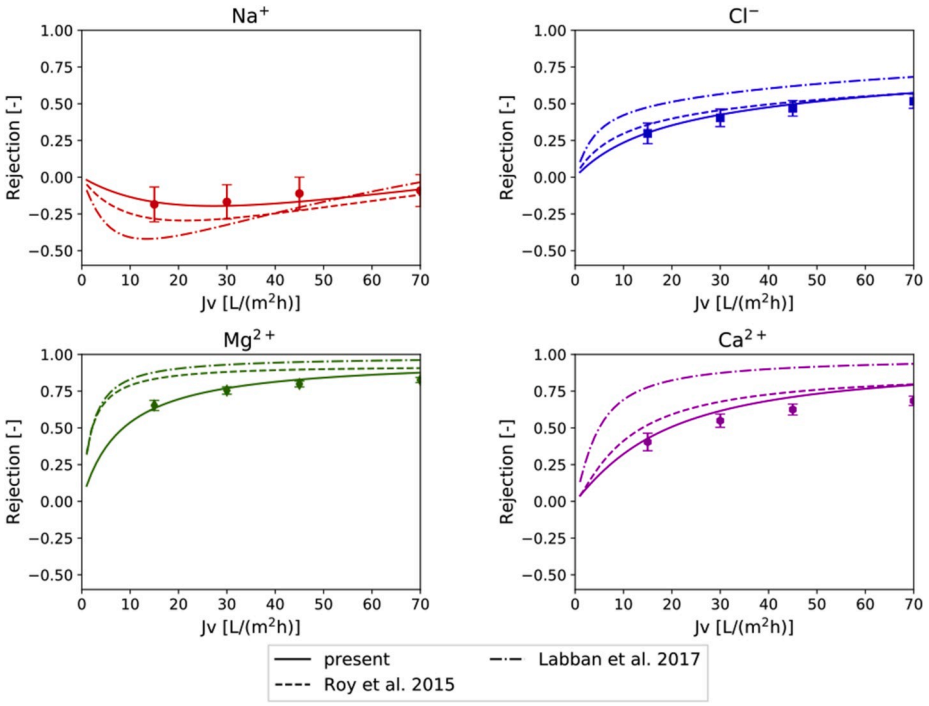

Fig. 12. Comparison of the ionic rejections calculated by the model for the brine solution with the parameters found in the present work and with the ones found for seawater in the works by Roy et al. and Labban et al.

a circular scheme in the water softening industry.

6. Conclusions

This study presents the characterization of NF membranes in the presence of a multi-ionic solution simulating the effluent produced by the regeneration of ion exchange resins employed for water softening. We performed experiments with two NF membranes and two solutions, the synthetic brine and a 10 times diluted brine, in a wide range of pH and permeate fluxes. Then, we found the four parameters to characterize the membranes by fitting the DSPM-DE to the experimental results. A good agreement between the experimental values and the simulated trends of ionic rejections vs. permeate flux was observed with errors lower than 15%. Finally, we analysed the trans-membrane fluxes and the exclusion coefficients given by the model.

Concerning the membrane parameters, we found negative values of membrane charge density and this could be explained by the high concentration of Cl^- in the feed, because Cl^- likely adsorbed onto the membrane surface and generated negatively charged sites. With diluted brine, higher ε_{pore} and higher (less negative) X_d were encountered because the water was less confined in the pores and because less Cl^- adsorption could take place. However, the trends of rejection obtained by varying the pH of the feed solutions were relatively flat and this suggested that, at the investigated concentrations, the membrane charge density did not affect the membrane performances significantly.

Generally speaking, the experimental rejections found with TS80 were always higher than the ones with NF270. This finding was supported by the lower ε_{pore} calculated for TS80, which corresponded to a stronger dielectric exclusion mechanism.

The analysis of the transmembrane fluxes of the divalent cations highlighted that the diffusive flux was the highest term in all cases. Moreover, the migrative flux decreased at lower concentrations and the Donnan exclusion term increased, because of the less negative membrane charge density. The convective flux with TS80 membranes was the only term that was slightly higher with the diluted brine because of a higher concentration of divalent ions in the membrane. This was because the dielectric exclusion mechanism played the most crucial role in the partition of the ions and it became weaker at lower concentrations.

Overall, the novel membrane parameters reported in this work allowed for simulating reliably two NF membranes in the presence of a multi-ionic solution reproducing the spent regenerant of ion exchange resins employed for water softening. Thus, the next step will consist in including them in full-scale models to design the NF plant to be employed for the treatment and recycling of the regeneration brine.

Credit author statement

Marina Micari: Conceptualization, Methodology, Software, Writing – Original Draft, Writing – Review and Editing; **Dionysia Diamantidou**: Investigation, Validation, Writing – Original Draft; **Bas Heijman**: Resources, Supervision; **Massimo Moser**: Methodology, Funding acquisition; **Amir Haidari**: Supervision, Writing – Review and Editing; **Henri Spanjers**: Writing – Review and Editing, Funding acquisition; **Valentin Bertsch**: Supervision, Writing – Review and Editing.

Declaration of competing interest

The authors declare that they have no known competing financial interests or personal relationships that could have appeared to influence the work reported in this paper.

Acknowledgments

This work was funded by the ZERO BRINE project (ZERO BRINE – Industrial Desalination – Resource Recovery – Circular Economy) - Horizon 2020 program, Project Number: 730390: www.zerobrine.eu.

Nomenclature

A	temperature correction factor for the activity coefficient [−]
C	concentration [mol/m^3]
$D_{i,pore}$	diffusion coefficient of the ion within the pore [m^2/s]
$D_{i,\infty}$	diffusion coefficient of the ion in the bulk [m^2/s]
e_0	electronic charge [1.602×10^{-19} C]
F	Faraday constant [9.64867×10^4 C/mol]
h_f	height of the NF feed channel [m]
I	ionic strength [mol/l]
j	trans-membrane flux [mol/(m^{2}s)]
J_v	permeate flux [m/s] or [L/(m^{2}h)]
$k^{bulk}_{c,i}$	mass transfer coefficient in the bulk [m/s]
$k^{,bulk}_{c,i}$	corrected mass transfer coefficient in the bulk [m/s]
k_B	Boltzmann constant [1.38066×10^{-23} J/K]
$k_{i,c}$	hindered convective mass transfer coefficient [−]
$k_{i,d}$	hindered diffusive mass transfer coefficient [−]
L_{mix}	mixing length of the spacer [m]
Lp	water permeability [L/(m^{2}h)/bar]
N	number of discretization elements within the membrane [−]
N_A	Avogadro number [6.023×10^{23} mol^{-1}]
P	pressure [Pa]
Pe	Peclet number [−]
R	ideal gas constant [8.314 J/(K mol)]
r_i	ion radius [nm]
R_i	ionic rejection [−]
r_p	pore radius [nm]
Sc	Schmidt number [−]
T	Temperature [K]
X_D	charge density [mol/m^3]
y	direction across the membrane from the feed to the permeate side [m]
z_i	valence of the ion [−]

Greek symbol

γ	activity coefficient [−]
δ_m	active layer membrane thickness [μm]
ΔP	net pressure difference [Pa]
$\Delta\Pi$	osmotic pressure difference [Pa]
$\Delta\psi_{D,feed}$	Donnan potential difference at the feed-membrane interface [V]
$\Delta\psi_{D,perm}$	Donnan potential difference at the permeate-membrane interface [V]
ΔW	Born solvation energy barrier [J]
ε	medium permittivity [F/m]
ε_0	vacuum permittivity [8.854×10^{-12} F/m]
ε_b	dielectric constant in the bulk [−]
ε_{pore}	pore dielectric constant [−]
η	solution viscosity [Pa s]
η_{mix}	mixing efficiency of the spacer [−]
λ_i	ratio between the ion Stokes radius and the pore radius [−]
ξ	electric potential gradient at the bulk-membrane interface [V/m]
Ξ	correction factor for the mass transfer coefficient [−]
Φ_i	steric coefficient [−]
Φ_B	Born solvation contribution for partitioning [−]
ψ	potential [V]

Subscripts

calc	calculated
exp	experimental
i	ion
j	index for the discretization along the NF membrane thickness
lim	limit

w	interface

Superscripts

b	bulk
bm	bulk-membrane interface
f	feed
m	membrane
p	permeate

Acronyms

DSPM	Donnan Steric Pore Model
DSPM-DE	Donnan Steric Pore Model with Dielectric Exclusion
MPD	m-phenylenediamine
MW	Molecular Weight [g/mol]
MWCO	Molecular Weight Cut-Off
NF	Nanofiltration
PIP	Piperazine
RO	Reverse Osmosis
SSE	sum of the squared errors [−]
TMC	trimesoyl chloride
TOC	Total Organic Carbon

References

[1] P. Eriksson, Nanofiltration extends the range of membrane filtration, Environ. Prog. 7 (1988) 58–62.
[2] N. Hilal, H. Al-Zoubi, N.A. Darwish, A.W. Mohamma, M. Abu Arabi, A comprehensive review of nanofiltration membranes:Treatment, pretreatment, modelling, and atomic force microscopy, Desalination 170 (2004) 281–308.
[3] D.L. Oatley, L. Llenas, R. Perez, P.M. Williams, X. Martinez-Llado, M. Rovira, Review of the dielectric properties of nanofiltration membranes and verification of the single oriented layer approximation, Adv. Colloid Interface Sci. 173 (2012) 1–11.
[4] A. Escoda, S. Déon, P. Fievet, Assessment of dielectric contribution in the modeling of multi-ionic transport through nanofiltration membranes, J. Membr. Sci. 378 (2011) 214–223.
[5] F. Salehi, S.M.A. Razavi, M. Elahi, Purifying anion exchange resin regeneration effluent using polyamide nanofiltration membrane, Desalination 278 (2011) 31–35.
[6] A.W. Mohammad, Y.H. Teow, W.L. Ang, Y.T. Chung, D.L. Oatley-Radcliffe, N. Hilal, Nanofiltration membranes review: recent advances and future prospects, Desalination 356 (2015) 226–254.
[7] F.F. Chang, W.J. Liu, X.M. Wang, Comparison of polyamide nanofiltration and low-pressure reverse osmosis membranes on As(III) rejection under various operational conditions, Desalination 334 (2014) 10–16.
[8] A. De Munari, A.J.C. Semiao, B. Antizar-Ladislao, Retention of pesticide endosulfan by nanofiltration: influence of organic matter-pesticide complexation and solute-membrane interactions, Water Res. 47 (2013) 3484–3496.
[9] M.A. Abdel-Fatah, Nanofiltration systems and applications in wastewater treatment: review article, Ain Shams Engineering Journal 9 (2018) 3077–3092.
[10] Q. Li, Z. Liao, X. Fang, D. Wang, J. Xie, X. Sun, L. Wang, J. Li, Tannic acid-polyethyleneimine crosslinked loose nanofiltration membrane for dye/salt mixture separation, J. Membr. Sci. 584 (2019) 324–332.
[11] M. Jiang, K. Ye, J. Lin, Y. Zhang, W. Ye, S. Zhao, B. Van der Bruggen, Effective dye purification using tight ceramic ultrafiltration membrane, J. Membr. Sci. 566 (2018) 151–160.
[12] I. Koyuncu, Reactive dye removal in dye/salt mixtures by nanofiltration membranes containing vinylsulphone dyes: effects of feed concentration and cross flow velocity, Desalination 143 (2002) 243–253.
[13] J.M. Gozálvez-Zafrilla, D. Sanz-Escribano, J. Lora-García, M.C. León Hidalgo, Nanofiltration of secondary effluent for wastewater reuse in the textile industry, Desalination 222 (2008) 272–279.
[14] B. Van der Bruggen, B. Daems, D. Wilms, C. Vandecasteele, Mechanisms of retention and flux decline for the nanofiltration of dye baths from the textile industry, Separ. Purif. Technol. 22–23 (2001) 519–528.
[15] S.S. Wadekar, R.D. Vidic, Insights into the rejection of barium and strontium by nanofiltration membrane from experimental and modeling analysis, J. Membr. Sci. 564 (2018) 742–752.
[16] Z.V.P. Murthy, L.B. Chaudhari, Separation of binary heavy metals from aqueous solutions by nanofiltration and characterization of the membrane using Spiegler–Kedem model, Chem. Eng. J. 150 (2009) 181–187.
[17] C.-V. Gherasim, P. Mikulášek, Influence of operating variables on the removal of heavy metal ions from aqueous solutions by nanofiltration, Desalination 343 (2014) 67–74.
[18] Y. Li, Y. Zhao, H. Wang, M. Wang, The application of nanofiltration membrane for recovering lithium from salt lake brine, Desalination (2019) 468.
[19] X. Chen, T. Chen, J. Li, M. Qiu, K. Fu, Z. Cui, Y. Fan, E. Drioli, Ceramic nanofiltration and membrane distillation hybrid membrane processes for the purification and recycling of boric acid from simulative radioactive waste water, J. Membr. Sci. 579 (2019) 294–301.
[20] S.S. Wadekar, R.D. Vidic, Comparison of ceramic and polymeric nanofiltration membranes for treatment of abandoned coal mine drainage, Desalination 440 (2018) 135–145.
[21] J. Warczok, M. Ferrando, F. López, C. Güell, Concentration of apple and pear juices by nanofiltration at low pressures, J. Food Eng. 63 (2004) 63–70.
[22] Z. Chen, J. Luo, X. Hang, Y. Wan, Physicochemical characterization of tight nanofiltration membranes for dairy wastewater treatment, J. Membr. Sci. 547 (2018) 51–63.
[23] F. Salehi, Current and future applications for nanofiltration technology in the food processing, Food Bioprod. Process. 92 (2014) 161–177.
[24] M.S. Noghabi, S.M.A. Razavi, S.M. Mousavi, M. Elahi, R. Niazmand, Effect of operating parameters on performance of nanofiltration of sugar beet press water, Procedia Food Science 1 (2011) 160–164.
[25] S. Wadley, C.J. Brouckaert, L.A.D. Baddock, C.A. Buckley, Modelling of nanofiltration applied to the recovery of salt from waste brine at a sugar decolourisation plant, J. Membr. Sci. 102 (1995) 163–175.
[26] W.L. Ang, A.W. Mohammad, N. Hilal, C.P. Leo, A review on the applicability of integrated/hybrid membrane processes in water treatment and desalination plants, Desalination 363 (2015) 2–18.
[27] D. Zhou, L. Zhu, Y. Fu, M. Zhu, L. Xue, Development of lower cost seawater desalination processes using nanofiltration technologies — a review, Desalination 376 (2015) 109–116.
[28] L. Llenas, X. Martínez-Lladó, A. Yaroshchuk, M. Rovira, J. de Pablo, Nanofiltration as pretreatment for scale prevention in seawater reverse osmosis desalination, Desalination and Water Treatment 36 (2012) 310–318.
[29] A.A. Al-Hajouri, A.S. Al-Amoudi, A.M. Farooque, Long term experience in the operation of nanofiltration pretreatment unit for seawater desalination at SWCC SWRO plant, Desalination and Water Treatment 51 (2013) 1861–1873.
[30] M.A.K. Al-Sofi, Seawater desalination - SWCC experience and vision, Desalination 135 (2001) 121–139.
[31] M.A.K. Al-Sofi, A.M. Hassan, G.M. Mustafa, A.G.I. Dalvi, N.M. Kither, Nanofiltration as a means of achieving higher TBT of $\geq 120^{\circ}$C in MSF, Desalination 118 (1998) 123–129.
[32] M. Kabsch-Korbutowicz, J. Wisniewski, S. Łakomska, A. Urbanowska, Application of UF, NF and ED in natural organic matter removal from ion-exchange spent regenerant brine, Desalination 280 (2011) 428–431.
[33] European Commission, Communication from the Commission to the European Parliament, the Council, the European Economic and Social Committe and the Committe of the Regions on the 2017 List of Critical Raw Materials for the EU, 2017.
[34] M. Micari, A. Cipollina, A. Tamburini, M. Moser, V. Bertsch, G. Micale, Combined membrane and thermal desalination processes for the treatment of ion exchange resins spent brine, Appl. Energy (2019) 254.
[35] S. Singh, K.C. Khulbe, T. Matsuura, P. Ramamurthy, Membrane characterization by solute transport and atomic force microscopy, J. Membr. Sci. 142 (1998) 111–127.
[36] M. Ernst, A. Bismarck, J. Springer, M. Jekel, Zeta-potential and rejection rates of a polyethersulfone nanofiltration membrane in single salt solutions, J. Membr. Sci. 165 (2000) 251–259.
[37] W.R. Bowen, A.W. Mohammad, N. Hilal, Characterisation of nanofiltration membranes for predictive purposes use of salts, uncharged solutes and atomic force microscopy, J. Membr. Sci. 126 (1997) 91–105.
[38] K.S. Spiegler, O. Kedem, Thermodynamics of hyperfiltration (reverse osmosis): criteria for efficient membranes, Desalination 1 (1966) 311–326.
[39] T. Tsuru, S.I. Nakao, S. Kimura, Calculation of ion rejection by extended Nernst-Planck equation with charged reverse osmosis membranes for single and mixed electrolyte solutions, J. Chem. Eng. Jpn. 24 (1991) 511–517.
[40] X.L. Wang, T. Tsuru, S.I. Nakao, S. Kimura, Electrolyte transport through nanofiltration membranes by the space-charge model and the comparison with Teorell- Meyer-Sievers model, J. Membr. Sci. 103 (1995) 117–133.
[41] D. Vezzani, S. Bandini, Donnan equilibrium and dielectric exclusion for of nanofiltration membranes, Desalination 149 (2002) 477–483.
[42] A.W. Mohammad, N. Hilal, H. Al-Zoubi, N.A. Darwish, Prediction of permeate fluxes and rejections of highly concentrated salts in nanofiltration membranes, J. Membr. Sci. 289 (2007) 40–50.
[43] C. Mazzoni, L. Bruni, S. Bandini, Nanofiltration: role of the electrolyte and pH on desal DK performances, Ind. Eng. Chem. Res. 46 (2007) 2254–2262.
[44] A.A. Hussain, S.K. Nataraj, M.E.E. Abashar, I.S. Al-Mutaz, T.M. Aminabhavi, Prediction of physical properties of nanofiltration membranes using experiment and theoretical models, J. Membr. Sci. 310 (2008) 321–336.
[45] N.S. Kotrappanavar, A.A. Hussain, M.E.E. Abashar, I.S. Al-Mutaz, T. M. Aminabhavi, M.N. Nadagouda, Prediction of physical properties of nanofiltration membranes for neutral and charged solutes, Desalination 280 (2011) 174–182.
[46] V. Silva, V. Geraldes, A.M. Brites Alves, L. Palacio, P. Prádanos, A. Hernández, Multi-ionic nanofiltration of highly concentrated salt mixtures in the seawater range, Desalination 277 (2011) 29–39.
[47] S. Déon, P. Dutournié, L. Limousy, P. Bourseau, Transport of salt mixtures through nanofiltration membranes: numerical identification of electric and dielectric contributions, Separ. Purif. Technol. 69 (2009) 225–233.
[48] Y. Roy, M.H. Sharqawy, J.H. Lienhard, Modeling of flat-sheet and spiral-wound nanofiltration configurations and its application in seawater nanofiltration, J. Membr. Sci. 493 (2015) 360–372.

[49] O. Labban, C. Liu, T.H. Chong, J.H. Lienhard V, Fundamentals of low-pressure nanofiltration: membrane characterization, modeling, and understanding the multi-ionic interactions in water softening, J. Membr. Sci. 521 (2017) 18–32.
[50] D.L. Oatley, L. Llenas, N.H.M. Aljohani, P.M. Williams, X. Martínez-Lladó, M. Rovira, J. de Pablo, Investigation of the dielectric properties of nanofiltration membranes, Desalination 315 (2013) 100–106.
[51] J.V. Nicolini, C.P. Borges, H.C. Ferraz, Selective rejection of ions and correlation with surface properties of nanofiltration membranes, Separ. Purif. Technol. 171 (2016) 238–247.
[52] M. Teixeira, M. Rosa, M. Nystrom, The role of membrane charge on nanofiltration performance, J. Membr. Sci. 265 (2005) 160–166.
[53] R. Epsztein, E. Shaulsky, N. Dizge, D.M. Warsinger, M. Elimelech, Role of ionic charge density in donnan exclusion of monovalent anions by nanofiltration, Environ. Sci. Technol. 52 (2018) 4108–4116.
[54] S.S. Wadekar, R.D. Vidic, Influence of active layer on separation potentials of nanofiltration membranes for inorganic ions, Environ. Sci. Technol. 51 (2017) 5658–5665.
[55] P. Dechadilok, W.M. Deen, Hindrance factors for diffusion and convection in pores, Ind. Eng. Chem. Res. 45 (2006) 6953–6959.
[56] F.G. Donnan, Theory of membrane equilibria and membrane potentials in the presence of non-dialysing electrolytes. A contribution to physical-chemical physiology, J. Membr. Sci. 100 (1995) 45–55.
[57] D.L. Parkhurst, C. Appelo, User's Guide to PHREEQC (Version 2): A Computer Program for Speciation, Batch-Reaction, One-Dimensional Transport and Inverse Geochemical Calculations, 2008.
[58] M. Born, Volumen und Hydratationswärme der Ionen, Z. Phys. Chem. 1 (1920).
[59] V. Geraldes, M.D. Afonso, Generalized mass-transfer correction factor for nanofiltration and reverse osmosis, AIChE J. 52 (2006) 3353–3362.
[60] S. Senthilmurugan, A. Ahluwalia, S.K. Gupta, Modeling of a spiral-wound module and estimation of model parameters using numerical techniques, Desalination 173 (2005) 269–286.
[61] V. Geraldes, A.M. Brites Alves, Computer program for simulation of mass transport in nanofiltration membranes, J. Membr. Sci. 321 (2008) 172–182.
[62] M. Mullett, R. Fornarelli, D. Ralph, Nanofiltration of mine water: impact of feed pH and membrane charge on Resource recovery and water discharge, Membranes 4 (2014) 163–180.
[63] J. Schaep, C. Vandecasteele, A.W. Mohammad, W.R. Bowen, Analysis of the salt retention of nanofiltration membranes using the donnan–steric partitioning pore model, Separ. Sci. Technol. 34 (1999) 3009–3030.
[64] Dow Water and Process Solutions, Filmtec Reverse Osmosis Membrane, Technical Manual, 2018.
[65] S.I. Nakao, S. Kimura, Analysis of solutes rejection in ultrafiltration, J. Chem. Eng. Jpn. 14 (1981) 32–37.
[66] J. Schaep, B. Van der Bruggen, C. Vandecasteele, D. Wilms, Influence of ion size and charge in nanofiltration, Separ. Purif. Technol. 14 (1998) 155–162.
[67] Y.L. Lin, P.C. Chiang, E.E. Chang, Removal of small trihalomethane precursors from aqueous solution by nanofiltration, J. Hazard Mater. 146 (2007) 20–29.
[68] M. Dalwani, N.E. Benes, G. Bargeman, D. Stamatialis, M. Wessling, Effect of pH on the performance of polyamide/polyacrylonitrile based thin film composite membranes, J. Membr. Sci. 372 (2011) 228–238.
[69] S. Déon, A. Escoda, P. Fievet, P. Dutournié, P. Bourseau, How to use a multi-ionic transport model to fully predict rejection of mineral salts by nanofiltration membranes, Chem. Eng. J. 189–190 (2012) 24–31.
[70] Y. Roy, D.M. Warsinger, J.H. Lienhard, Effect of temperature on ion transport in nanofiltration membranes: diffusion, convection and electromigration, Desalination 420 (2017) 241–257.
[71] G. Hagmeyer, R. Gimbel, Modelling the salt rejection of nanofiltration membranes for ternary ion mixtures and for single salts at different pH values, Desalination 117 (1998) 247–256.
[72] B.W. Su, X.J. Duan, M.W. Dou, X.L. Gao, C.J. Gao, Charge characteristics of nanofiltration membrane by streaming potential method, Adv. Mater. Res. 396–398 (2011) 547–551.
[73] D.-X. Wang, M. Su, Z.-Y. Yu, X.-L. Wang, M. Ando, T. Shintani, Separation performance of a nanofiltration membrane influenced by species and concentration of ions, Desalination 175 (2005) 219–225.
[74] K. Zhao, G. Ni, Dielectric analysis of nanofiltration membrane in electrolyte solutions: influences of permittivity of wet membrane and volume charge density on ion permeability, J. Electroanal. Chem. 661 (2011) 226–238.